

Electronic Supplementary Information of

The dependence of new particle formation rates on the interaction between cluster growth, evaporation, and condensation sink

Chenxi Li¹, Yue Zhao¹, Ziyue Li¹, Ling Liu², Xiuhui Zhang², Jun Zheng³, Veli-matti Kerminen⁴, Markku
Kulmala^{4,5}, Jingkun Jiang⁶, Runlong Cai^{*4}, Huayun Xiao^{*1}

¹School of Environmental Science and Engineering, Shanghai Jiao Tong University, 200240, Shanghai, China

²Key Laboratory of Cluster Science, Ministry of Education of China, School of Chemistry and Chemical Engineering,
Beijing Institute of Technology, Beijing 100081, China

³Collaborative Innovation Center of Atmospheric Environment and Equipment Technology, Nanjing University of
Information Science & Technology, Nanjing, 210044, China

⁴Institute for Atmospheric and Earth System Research / Physics, Faculty of Science, University of Helsinki, 00014
Helsinki, Finland

⁵Aerosol and Haze Laboratory, Beijing Advanced Innovation Center for Soft Matter Science and Engineering, Beijing
University of Chemical Technology, 100029 Beijing, China

⁶State Key Joint Laboratory of Environment Simulation and Pollution Control, School of Environment, Tsinghua
University, 100084 Beijing, China

**Correspondence to:* Runlong Cai (runlong.cai@helsinki.fi); Huayun Xiao (xiaohuayun@sjtu.edu.cn)

S1 Details of calculation for Fig. 2

In the simulation of cluster formation without evaporation, the monomer is assumed to have a molecular weight of 98 g/mol and a density of 1830 kg/m³. The collision rates are calculated with the free molecular collision rate equation. An enhancement factor of 2.3 is applied to all the collision rates to account for long range Van der Waals interactions. The CS for the monomer and clusters are calculated by integrating the monomer/cluster's collision rates with an artificial distribution of background particles. The CS is then varied by scaling the distribution. The monomer concentration is held constant during the simulation. Clusters grow by both molecular addition and coagulation. The simulated NPF rate J_i is given by particle number concentration fluxes past cluster $i-1$. CS is assumed to be a constant for each simulation and it is not affected by the contribution from newly formed particles

In the application of eqn (4), the collision rates and cluster specific CS are the same as in the simulation.

S2 Relative contribution of coagulation to NPF rates in the absence of evaporation

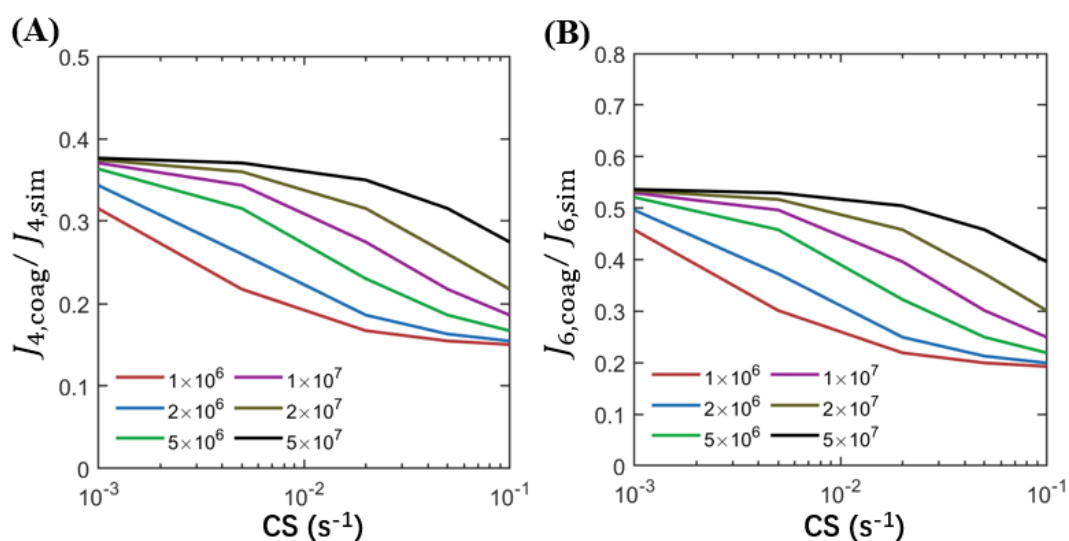


Figure S1. The fraction of coagulation-induced NPF rates in the simulation for J_4 (A) and J_6 (B)

From the simulation of the cluster formation (section 2.1 in the main text), the NPF rate contributed by cluster-cluster coagulation is directly retrievable. Figure S1 shows the ratio of coagulation induced particle formation to the total particle formation rates at the same simulation conditions as Fig. 2. Figure S1 reveals several trends. First of all, a comparison of Fig. S1B to S1A shows that coagulation contributes more to J_6 than J_4 . This is as expected since there are more possible particle formation channels by coagulation when the NPF rate is defined at a larger cluster size. Second, at a given CS value, higher vapor concentration leads to a higher fraction of particle formation by coagulation. Third, at a given monomer concentration, the contribution of coagulation to the NPF rates decreases as

CS increases.

S3 Exact solution for J_5

For cluster i , we define $X_i = CS_i + E_i + k_i$. If cluster 5 is stable and its evaporation can be neglected, the relation between n_4 and n_1 can be derived by solving eqns (6) and (7) in the main text. n_4 is expressed by:

$$n_4 = \frac{k_1 n_1}{\frac{X_2 X_3 X_4}{k_2 k_3} \frac{E_4 X_2}{k_2} \frac{E_3 X_4}{k_3}} \quad (\text{S2})$$

J_5 is then given by

$$J_5 = k_4 n_4 = \frac{k_1 n_1}{\frac{X_2 X_3 X_4}{k_2 k_3 k_4} \frac{E_4 X_2}{k_2 k_4} \frac{E_3 X_4}{k_3 k_4}} \quad (\text{S3})$$

S4 Errors of eqn (12) for a homo-molecular NPF system

We compared the exact solutions of J_4 and J_5 (eqn (9) and eqn S3) with the approximate solution given by eqn (12). The error of the approximate solution was calculated by $|J_{\text{approx}} - J_{\text{exact}}|/J_{\text{exact}}$. In doing these calculations, we varied CS_1, E_2, E_3, n_1 for J_4 and varied CS_1, E_2, E_3, E_4, n_1 for J_5 . The collision rate coefficient for two monomers was set to $0.25 \times 10^9 \text{ cm}^3 \text{ s}^{-1}$, which considers double counting when two identical entities collide. Other collision rate coefficients were assumed to scale with $\left(1 + \frac{1}{i}\right)^{\frac{1}{2}} \left(1 + i^{\frac{1}{3}}\right)^2$ and CS_i was set to be inversely proportional to \sqrt{i} (i is the cluster size).

Figure S1 shows the error of $J_{4,\text{approx}}$ for the following conditions: $CS_1 = 0.002 \text{ s}^{-1}, 0.02 \text{ s}^{-1}, 0.2 \text{ s}^{-1}$; $E_2 = 0.02 \text{ s}^{-1}, 0.2 \text{ s}^{-1}, 1 \text{ s}^{-1}$; $n_1 = 1 \times 10^6 - 5 \times 10^8 \text{ cm}^{-3}$; $E_3 = 0 - E_2$. These conditions cover the typical values of CS and evaporation rates relevant to NPF in the atmospheric boundary layer. Figure S1 shows that the error does not exceed 25% at these conditions.

Figure S2 shows the error of $J_{5,\text{approx}}$ for the following conditions: $CS_1 = 0.002 \text{ s}^{-1}, 0.02 \text{ s}^{-1}, 0.2 \text{ s}^{-1}$; $E_2 = 0.02 \text{ s}^{-1}, 0.2 \text{ s}^{-1}, 1 \text{ s}^{-1}$; $n_1 = 1 \times 10^6 - 5 \times 10^8 \text{ cm}^{-3}$; $E_3 = E_2$; $E_4 = 0 - E_3$. Figure S2 shows that the error does not exceed 45% at these conditions. We further varied E_3 from 0 to E_2 and found that the maximum error does not exceed 45% (results not shown).

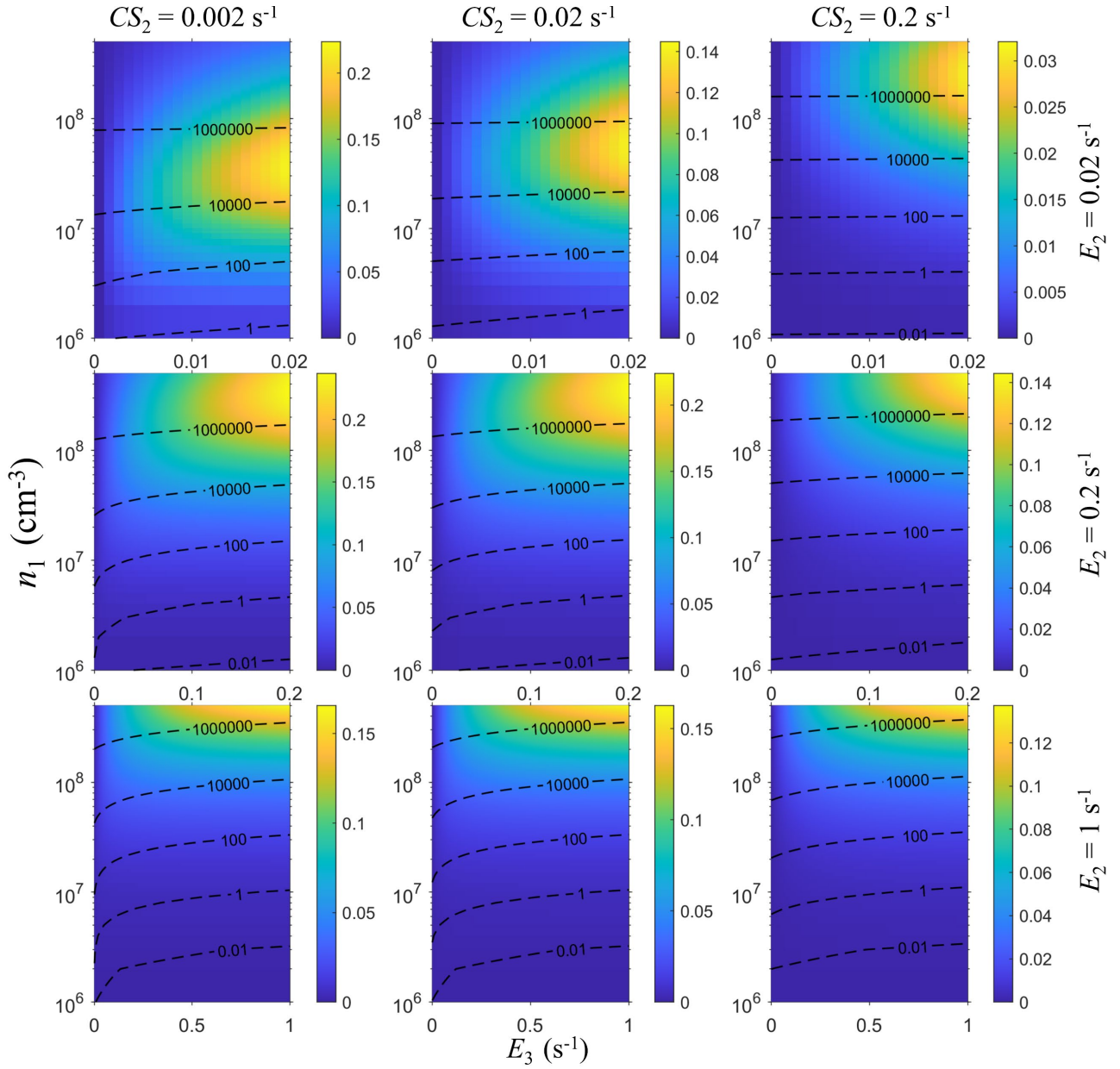


Figure S2. The error of J_4 calculated by eqn (12) compared to the exact solution calculated by eqn (9). The color bar shows the value of $|J_{4,\text{eqn } 12} - J_{4,\text{eqn } 9}|/J_{4,\text{eqn } 9}$. The CS_1 and E_2 values for each subplot are shown on the top and right of the figure. Contour lines show the value of $J_{4,\text{eqn } 9}$.

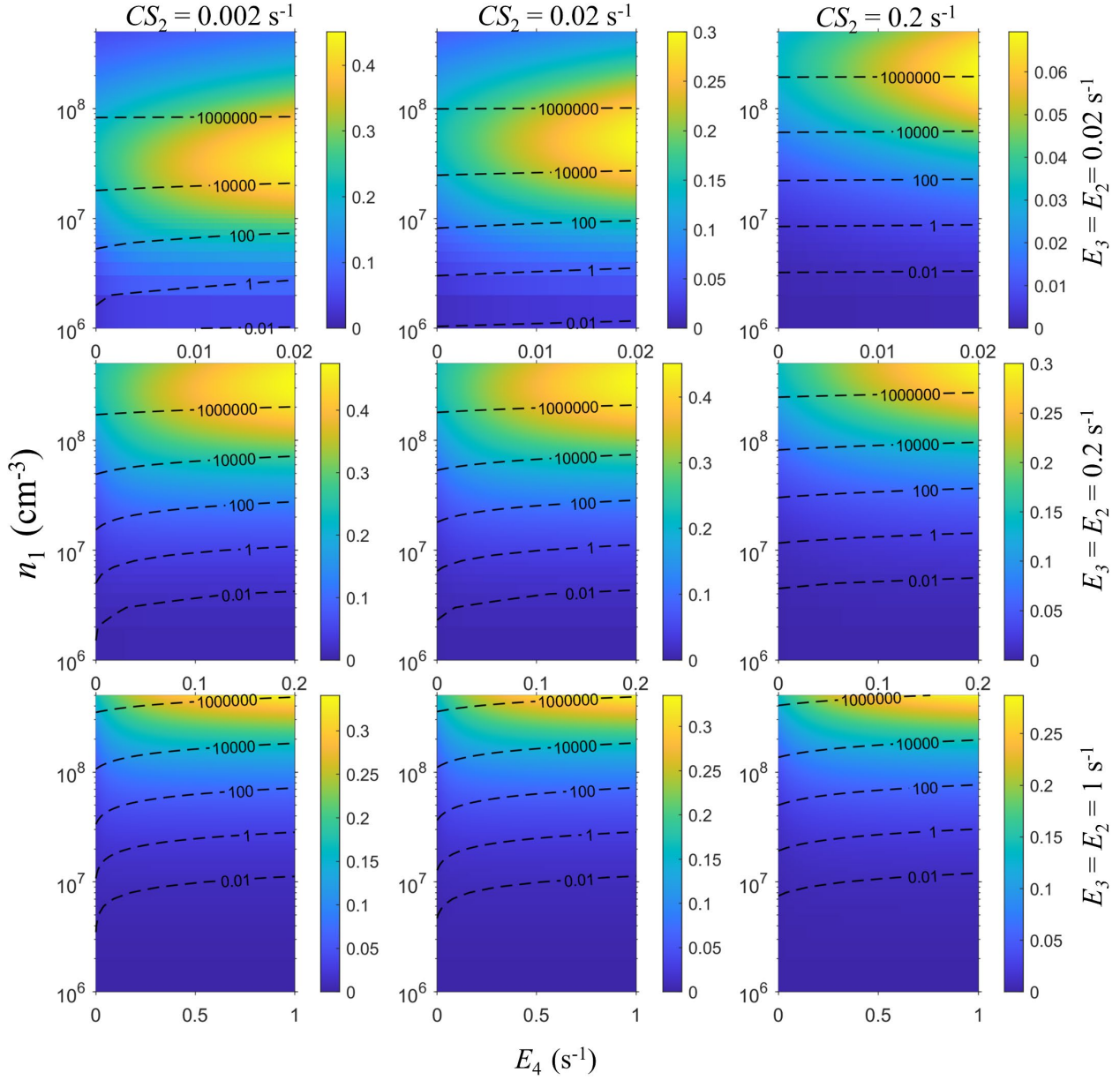


Figure S3. The error of J_5 calculated by eqn (12) compared to the exact solution calculated by eqn (S3). The color bar shows the value of $|J_{5,\text{eqn 12}} - J_{5,\text{eqn S3}}|/J_{5,\text{eqn S3}}$. The CS_1 , E_2 and E_3 values for each subplot is labelled on the top and right of the figure. Contour lines show the value of $J_{5,\text{eqn S3}}$.

S5 NPF by coagulation in the test cases

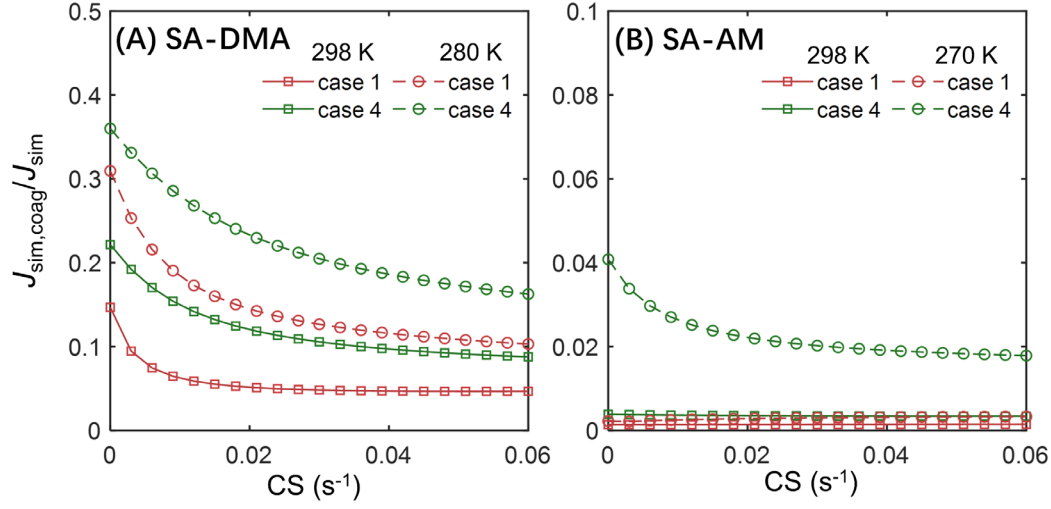


Figure S4. The fraction of NPF by cluster coagulation in the lowest NPF rate scenario (case 1) and the highest NPF rate scenario (case 4) for both the SA-DMA nucleation (A) and the SA-AM nucleation (B). Two temperatures are shown for both the SA-DMA and the SA-AM nucleation. The simulation conditions can be found in Table 1 in the main text.

S6 Calculation of cluster evaporation rates of the SA_iAM_j clusters

The weights of the SA_iAM_j clusters, f_{ij} 's are calculated assuming that clusters containing the same number of SA molecules, but different number of AM molecules are at equilibrium concentration. The fraction of SA_iAM_j clusters is given by

$$f_{i1} = \frac{1}{1 + \frac{k_{i1}}{E_{i2}} + \frac{k_{i1}k_{i2}}{E_{i2}E_{i3}} + \dots + \frac{\prod_{x=1}^{i-1} k_{ix}}{\prod_{x=2}^i E_{ix}}} \quad (S4)$$

and

$$f_{ij} = \frac{\frac{\prod_{x=1}^{j-1} k_{ix}}{\prod_{x=2}^j E_{ix}}}{1 + \frac{k_{i1}}{E_{i2}} + \frac{k_{i1}k_{i2}}{E_{i2}E_{i3}} + \dots + \frac{\prod_{x=1}^{i-1} k_{ix}}{\prod_{x=2}^i E_{ix}}} \quad (j \geq 2) \quad (S5)$$

where k_{ix} is the collision rate between SA_iAM_x with an ammonia molecule and E_{ix} is the evaporation rate of an ammonia molecule from an SA_iAM_x cluster. Note that in the calculation of f_{ij} , we have only considered cluster containing 1 to i ammonia molecules. Pure SA clusters and cluster with more base than acid molecules contribute negligibly to the cluster number concentrations.

S7 Cluster evaporation rates of SA₃DMA₂ and SA₄DMA₃

70 **Table S1.** Evaporation rates (s⁻¹) of SA₁ from SA₃DMA₂ and SA₄DMA₃ at 298 K. In the calculation of the evaporation rates, the collision rate coefficients of SA₁ with SA₂DMA₂ and SA₃DMA₂ are set to 1.12×10⁻⁹ cm³ s⁻¹ and 1.27×10⁻⁹ cm³ s⁻¹, respectively. These collision rate coefficients are 2.3 times higher than the hard sphere collision coefficients to account for collision enhancement due to long range interactions between colliding entities.

Source	SA ₃ DMA ₂ → SA ₂ DMA ₂ +SA ₁	SA ₄ DMA ₃ → SA ₃ DMA ₃ +SA ₁
Li et al. ¹	0.0428	0.1501
Myllys et al. ²	0.0440	18.5745
Ortega et al. ³	8.0362	0.2414

75 S8 Derivation of eqns (15), (18) and (19)

Recall that [SA]_t is the combined concentration of SA₁ and SA₁DMA₁. We consider how [SA]_t is distributed between SA₁ and SA₁DMA₁. Neglecting coagulation with other clusters as well as SA₁DMA₁ formation due to the evaporation of larger clusters, the balance equation for SA₁DMA₁ at steady state is

$$n_{SA}n_{DMA}\beta_{SA-DMA} = n_{SA_1DMA_1}(E_1 + CS_1 + k_1). \quad (S6)$$

80 Since k_1 is much lower than E_1+CS_1 for most conditions (see Table 1 for the values of E_1),

$$n_{SA_1DMA_1} = n_{SA}n_{DMA} \frac{\beta_{SA-DMA}}{E_1+CS_1} = n_{SA} \frac{k_0}{E_1+CS_1}. \quad (S7)$$

Using the relation $n_t = n_{SA} + n_{SA_1DMA_1}$,

$$n_{SA} = \frac{n_t(E_1+CS_1)}{k_0 + E_1+CS_1} \quad (S8) \text{ or } (14)$$

$$n_{SA_1DMA_1} = \frac{n_t k_0}{k_0 + E_1+CS_1} \quad (S9)$$

85 Combining eqn (S6) and eqn (12), we have

$$J = k_1 n_t \frac{E_1+CS_1}{k_0 + E_1+CS_1} \prod_{i=1}^3 \frac{k_i}{k_i + CS_i + E_i} \quad (S10) \text{ or } (15)$$

To account for the instability of SA₄DMA₃ and SA₃DMA₂, we only need to modify the relevant cluster growth rates in eqn (S10). If SA₄DMA₃ is so unstable that it instantly evaporates, the cluster SA₃DMA₃ can only grow by the

addition of SA₁DMA₁, hence its growth rate should be $k'_3 = \beta_3 n_{SA_1DMA_1}$. Replacing k_3 in eqn (S10) by k'_3 and
 90 apply eqn (S9),

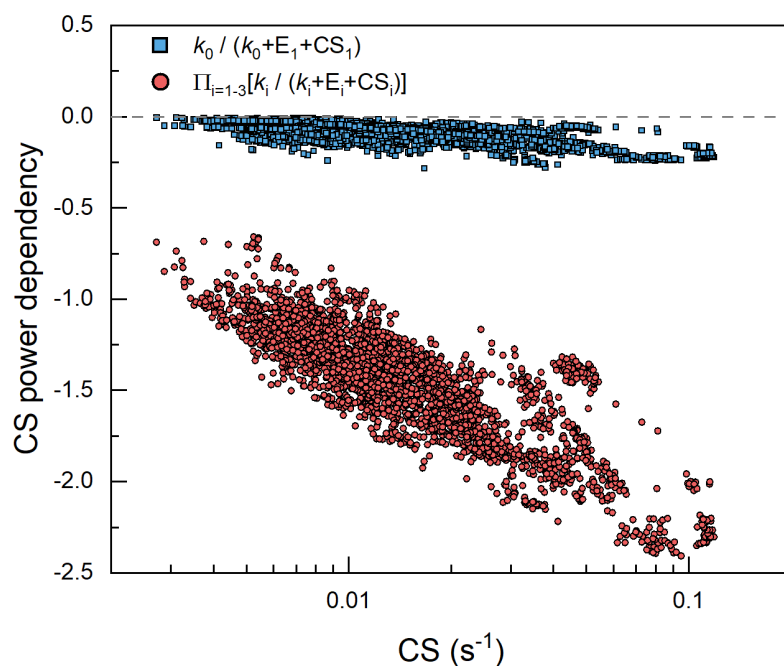
$$\begin{aligned}
 J &= k_0 n_t \frac{E_1 + CS_1}{k_0 + E_1 + CS_1} \left(\prod_{i=1}^2 \frac{k_i}{k_i + CS_i + E_i} \right) \frac{\beta_3 n_{SA_1DMA_1}}{k_3 + CS_3 + E_3} \\
 &= k_0 n_t \frac{E_1 + CS_1}{k_0 + E_1 + CS_1} \left(\prod_{i=1}^2 \frac{k_i}{k_i + CS_i + E_i} \right) \frac{\beta_3}{k_3 + CS_3 + E_3} \frac{n_t k_0}{k_0 + E_1 + CS_1} \\
 &= k_0 n_t \frac{E_1 + CS_1}{k_0 + E_1 + CS_1} \frac{k_0}{k_0 + E_1 + CS_1} \left(\prod_{i=1}^3 \frac{k_i}{k_i + CS_i + E_i} \right). \tag{S9} \text{ or } (16)
 \end{aligned}$$

To further account for the instability of SA₃DMA₂, we replace k_2 in eqn (S9) by $k'_2 = \beta_3 n_{SA_1DMA_1}$ and repeat the
 95 above procedure. This leads to

$$J = k_0 n_t \frac{E_1 + CS_1}{k_0 + E_1 + CS_1} \left(\frac{k_0}{k_0 + E_1 + CS_1} \right)^2 \prod_{i=1}^3 \frac{k_i}{k_i + CS_i + E_i}. \tag{S10} \text{ or } (17)$$

S9 CS dependency of different terms in eqns (15), (18) and (19)

Figure S3 compares the contribution of CS dependency from different terms in eqns (15), (18) and (19). These
 contributions are calculated by derivativizing $\log \left(\frac{k_0}{k_0 + E_1 + CS_1} \right)$ and $\log \left(\prod_{i=1}^3 \frac{k_i}{k_i + CS_i + E_i} \right)$ with respect to $\log(\text{CS})$
 100 while holding other variables (k_i 's and E_i 's) constant. Figure S3 shows that $\frac{k_0}{k_0 + E_1 + CS_1}$ has a power dependency on
 CS for no more than $\text{CS}^{-0.28}$ (blue squares; 10th percentile -0.03; median -0.08; 90th percentile -0.16) and hence
 $\left(\frac{k_0}{k_0 + E_1 + CS_1} \right)^{0-2}$ has a power dependency for no more than $\text{CS}^{-0.56}$. In contrast, the power dependency of
 $\prod_{i=1}^3 \frac{k_i}{k_i + CS_i + E_i}$ on CS is in the range of $\text{CS}^{-0.66}$ to $\text{CS}^{-2.4}$ (red circles; 10th percentile -1.1; median -1.4; 90th percentile -
 1.9).



105

Figure S5. Comparison of the CS power dependency of the term $\frac{k_0}{k_0 + E_1 + CS_1}$ (blue squares) and $\prod_{i=1}^3 \frac{k_i}{k_i + CS_i + E_i}$ (red circles) in eqns (15), (18) and (19).

References

- 110 1. H. Li, A. Ning, J. Zhong, H. Zhang, L. Liu, Y. Zhang, X. Zhang, X. C. Zeng and H. He, Influence of atmospheric conditions on sulfuric acid-dimethylamine-ammonia-based new particle formation, *Chemosphere*, 2020, **245**, 125554.
2. N. Myllys, S. Chee, T. Olenius, M. Lawler and J. Smith, Molecular-Level Understanding of Synergistic Effects in Sulfuric Acid–Amine–Ammonia Mixed Clusters, *J. Phys. Chem. A*, 2019, **123**, 2420-2425.
- 115 3. I. K. Ortega, O. Kupiainen, T. Kurtén, T. Olenius, O. Wilkman, M. J. McGrath, V. Loukonen and H. Vehkamäki, From quantum chemical formation free energies to evaporation rates, *Atmos. Chem. Phys.*, 2012, **12**, 225-235.